Nanoscale generation of white light for ultrabroadband nanospectroscopy

S.V. Makarov,[1] I.S. Sinev,[1] V.A. Milichko,[1] F.E. Komissarenko,[1]
D.A. Zuev,[1] E.V. Ushakova,[1] I.S. Mukhin,[1] Y.F. Yu,[2]
A.I. Kuznetsov,[2] P.A. Belov,[1] I.V. Iorsh,[1] A.N. Poddubny,[1,3]
A.K. Samusev,[1] Yu.S. Kivshar[1,4]

[1]ITMO University, St. Petersburg 197101, Russia,
[2]Data Storage Institute, A*STAR (Agency for Science, Technology and Research),
Fusionopolis Way 2, 08-01 Innovis, 138634, Singapore
[3]Ioffe Institute, St. Petersburg 194021, Russia
[4]Nonlinear Physics Center, Australian National University, Canberra ACT 2601, Australia

Achieving efficient localization of white light at the nanoscale is a major challenge due to the diffraction limit, and nanoscale emitters generating light with a broadband spectrum require complicated engineering. Here we suggest a simple, highly efficient nanoscale white-light source based on a hybrid Si/Au nanoparticle with ultrabroadband (1.3–3.4 eV) spectral characteristics. We incorporate this novel source into a scanning-probe microscope and observe broadband spectrum of photoluminescence that allows fast mapping of local optical response of advanced nanophotonic structures with submicron resolution, thus realizing *ultrabroadband near-field nanospectroscopy*.

Creation of efficient broadband nanoscale emitters operating at optical frequencies is a major fundamental challenge that is crucially important for many applications, including ultracompact optical chips, bioimaging, and active nanophotonics. An efficient nanoscale white-light source would be a powerful tool for nanospectroscopy (*1*), broadband probing of the near fields of nanophotonic devices or mapping their optical properties correlated with the local density of states (LDOS) (*2, 3*), as shown schematically in Fig. 1A.

Spectral maps of local optical properties *outside* nanostructures are usually measured by a near-field scanning optical microscope (NSOM) equipped with an optically active near-field probe (*4*). In this case, the near-field excitation of a nanostructure is provided by the emission of the subwavelength light source embedded in the probe, e.g. by quantum dots (*5*), active molecules (*6*), ions (*7*), or NV-centers (*8*). In general, all such probes suffer from a narrow spectral band (<100 nm) of the emitters. This problem is partially solved by using broadband supercontinuum sources in NSOM experiments with passive probes (*9*). This approach, however, revokes the opportunities for probing local density of states of nanophotonic structures, which is available for luminescent probes through measuring the changes in the decay rate (*10*).

Fundamental restrictions for the spectral broadening of photoluminescence (PL) of nanoscale emitters can be understood from a relation between the external quantum efficiency (EQE) η and spectral width $\Delta\omega$,

$$\eta = \frac{\xi\Gamma_r}{\Gamma_r + \Gamma_{nr}(\Delta\omega)}, \tag{1}$$

where Γ_r is the radiative rate, and ξ is the excitation efficiency. The nonradiative rate Γ_{nr} grows rapidly with the spectral width $\Delta\omega$ and quenches the quantum yield, e.g. due to the Arrhenius thermal activation of nonradiative channels, $\Gamma_{nr} \sim \exp\,[(\Delta\omega - E_0)/T]$, where *T* is temperature and E_0 is the ground state activation energy. Exponential suppression of the quantum yield for a broadband spectrum is a general trend for various types of nanoscale emitters, as illustrated schematically in Fig. 1B.

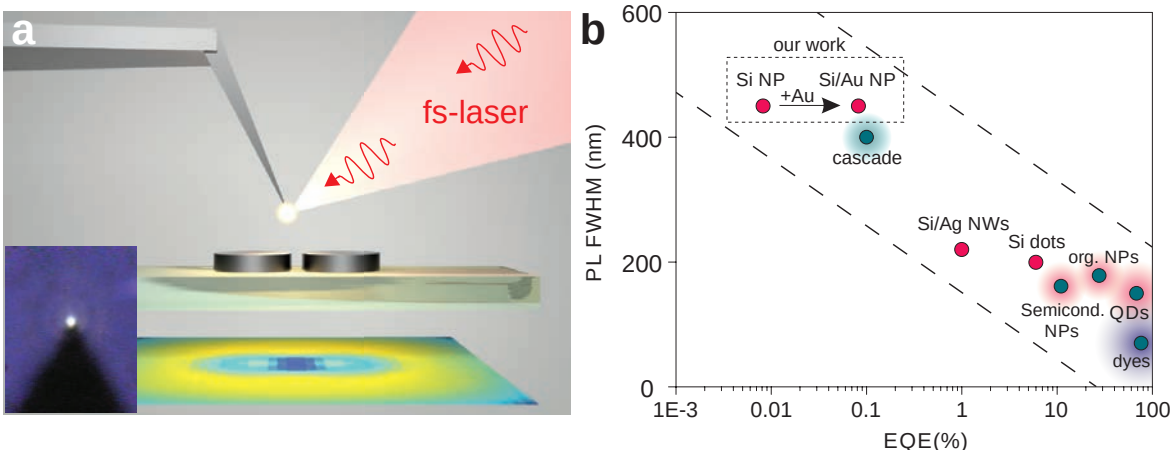

Figure 1: **Concept of a white-light source for ultrabroadband nanospectroscopy.** (**a**) A functionalized nanotip for ultrabroadband optical nanospectrometry. Inset: an optical image of the nanotip in experiment. (**b**) Summary of the external quantum efficiencies EQE (η) for photoluminiscence FWHM width for different subwavelength objects. Shaded area represents schematically the exponential decay of efficiency with an increase of the spectral width of emitted light. Abbreviations are: NP – nanoparticle, NW – nanowire, and QD – quantum dot. Corresponding references are summarized in Ref. (*15*).

One of the most promising materials for broadband PL is silicon (Si), that possesses direct and indirect optical bandgaps of 1.1 eV and 3.4 eV, respectively, and thus yields large values of $\Delta\omega\approx$2.3 eV. It was shown that Si nanoparticles demonstrate broadband photoluminescence (*11–14*). The problem of low efficiency of indirect radiative transitions can be solved by increasing Γ_r with the reduction of the size of Si crystallites (*11*), and by increasing the Purcell factor (*12*). However, small Si nanocrystals with higher quantum efficiency emit light in narrow bands, whereas high values of the Purcell factor require high-Q optical resonances implying again a narrow spectral response.

Here we report that a dramatic increase of the efficiency of the nanoscale white-light source can be achieved by *introducing gold (Au) islands into a Si nanoparticle* creating an unconventional type of metal-dielectric hybrid nanoparticle. We argue that gold inclusions play a pivotal role in the demonstrated outstanding performance of the white-light source because they boost

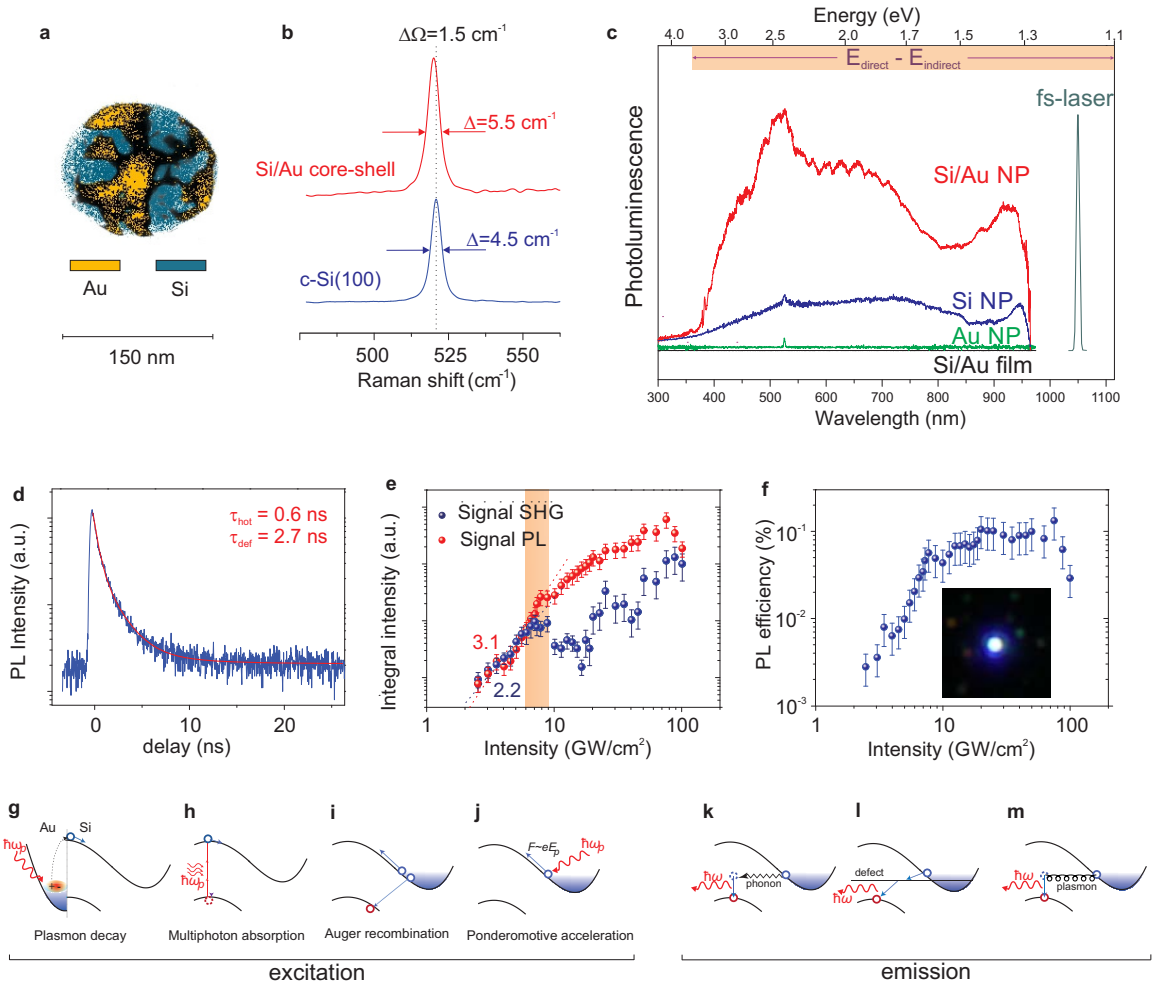

Figure 2: **Properties of hybrid Si/Au nanoparticles.** (**A**) TEM image and element composition of a 150-nm hybrid nanoparticle shown in false colors corresponding to Au (yellow) and Si (blue). (**B**) Raman spectra of the hybrid nanoparticle (red curve) and bulk crystalline Si (blue curve). (**C**) Measured photoluminescence spectra from a Si/Au nanoparticle (red curve), an Au nanoparticle (green curve), silicon nanoparticle (blue curve) and a two-layer a-Si:H/Au of thicknesses 15 nm/15 nm (black curve) at 50 GW/cm^2, spectrum of femtosecond laser pulses of the excitation (sea green curve). (**D**) Time-resolved PL signal from an individual hybrid nanoparticle excited with 405 nm diode picosecond laser. τ_{hot} and τ_{def} are decay times extracted after fitting of the experimental curve. (**E**) Dependences of photoluminescence (red dots) and second harmonic (blue dots) integral signals on the intensity of incident femtosecond laser pulses. The lines represent approximations by linear fits in double-log scale yielding 2.2- and 3.1-power slopes for blue and red dots, respectively. (**F**) Measured integral external power efficiency of photoluminescence from the hybrid nanoparticle at different intensities of excitation. The inset shows that the brightness of the hybrid nanoparticle (in very center) irradiated by focused (10× objective) fs-laser beam is much higher as compared to scattering signal from similar neighboring nanoparticles excited by white light from a halogen lamp with power 5 W focused by 10× objective at oblique incidence (65° angle of incidence, dark field configuration). (**G–J**) Schematic illustrations of the photoexcitation mechanisms. (**K–M**) Schematic illustrations of the emission mechanisms.

the photoexcitation efficiency ξ of the Si-based emitter by an order of magnitude making η around 0.1% via improved light absorption and photoinjection of hot electrons and holes into the active material. Furthermore, to demonstrate the potential of this novel white-light source for various applications in nanophotonics, we employ it to create an ultrabroadband active probe for nanospectroscopy.

To reveal the mechanisms behind the superior emission of hybrid nanoparticles fabricated by the laser ablation (see Ref. (*15*) for details), first we characterize their structure by employing the transmission electron microscopy (TEM) and Raman spectroscopy. Figure 2 summarizes the basic properties of Si/Au hybrid nanoparticles, revealing an island-type structure of the Au part [as shown in the TEM image in Fig. 2A] and polycrystalline structure of the Si part [see the Raman spectrum in Fig. 2B]. The resulting partially recrystallized material has an average grain size of about $d \sim$ 5–10 nm, in accord with the formula $d = 2\pi(B/\Delta\Omega)^{1/2}$, where $\Delta\Omega \approx 1.50 \pm 0.5$ cm^{-2} is the peak shift for nanocrystalline Si as compared with that of c-Si, and $B \approx 2$ cm^{-2} (*16*).

Figure 2C compares the emission spectra from different materials and structures upon irradiation by fs laser pulses (λ = 1050 nm or 1.18 eV, τ = 150 fs) with intensity 50 GW/cm^2. Details of nonlinear optical experiments are given in Ref. (*15*). Au nanoparticles as well as Au/Si film exhibit only a weak second-harmonic generation (SHG) signal around 525 nm. Relatively weak PL signal is usually observed from a-Si:H films, being centered around 650 nm that is caused by a direct bandgap at 1.8 eV in amorphous hydrogenated silicon (*17*). The PL spectrum of the a-Si:H film becomes much broader and intense after laser annealing (visible damage). Even better signal is achieved from a 300 nm Si particle fabricated from the 50-nm a-Si:H film by the laser printing method (*15*). Finally, the spectrum of a 150 nm hybrid nanoparticle fabricated from 15/60 nm Au/Si film is extremely strong, and it covers the entire visible spectrum with a characteristic white-color PL emission, see the inset in Fig. 1A. Taking into account the volume

difference, we estimate the efficiency of hybrid nanoparticles to be at least 20 times higher than that of Si nanoparticles (*15*).

Since there exists no decisive difference in the shape of the PL spectra of hybrid and pure Si nanoparticles, we conclude that there is no direct contribution to the PL signal from gold in the studied hybrid nanoparticles (Fig. 2C). Therefore, both bulk crystalline (*12*) and nanocrystalline (*11*) fractions govern the PL processes, while additional PL enhancement in the presence of Au part around Si originates from hot carriers photoinjection (*18, 19*). Taking into account two-exponent decay of the PL signal (see Fig. 2D) and three-photon mechanism of the PL excitation in the range of 2–10 GW/cm^2 (see Fig. 2E), the high PL yield (Fig. 2F) suggests an efficient cascade of hot carrier generation and radiative recombination processes. Responsible microscopic mechanisms are illustrated in Fig. 2G to Fig. 2M, which represent several scenarios for the PL generation discussed below.

First, three-photon absorption in gold (*20*) is known to be more efficient than that in Si (Figs. 2G,H), and it generates hot electrons with the energies up to $3h\nu + U \approx 4$ eV, where $h\nu$ is the energy of one fs laser photon (1.18 eV) and $U \approx 0.5$ eV is the Schottky barrier for the Si/Au contact. Also, the d-band of gold lies at -2.25 eV under the Fermi level, requiring 2 or 3 photons with energies 1.18 eV to induce the *d-s* transitions and generate hot holes. In parallel with absorption in gold via real states in *s*-band, multiphoton absorption in silicon occurs with much less probability via virtual states in the band gap.

Second, the generated hot electrons possessing high enough energy ($>$3.4 eV) are injected into conductance band of Si, as well as hot holes are injected into its valence band (*19*), as schematically shown in Fig.S8 (*15*).

Third, the hot electron-hole pairs relax nonradiatively and recombine by emitting photons. Observed broadband stationary emission indicates efficient PL of hot charge carriers. This is quite challenging for bulk silicon due to its indirect band gap nature, that makes phonon-assisted

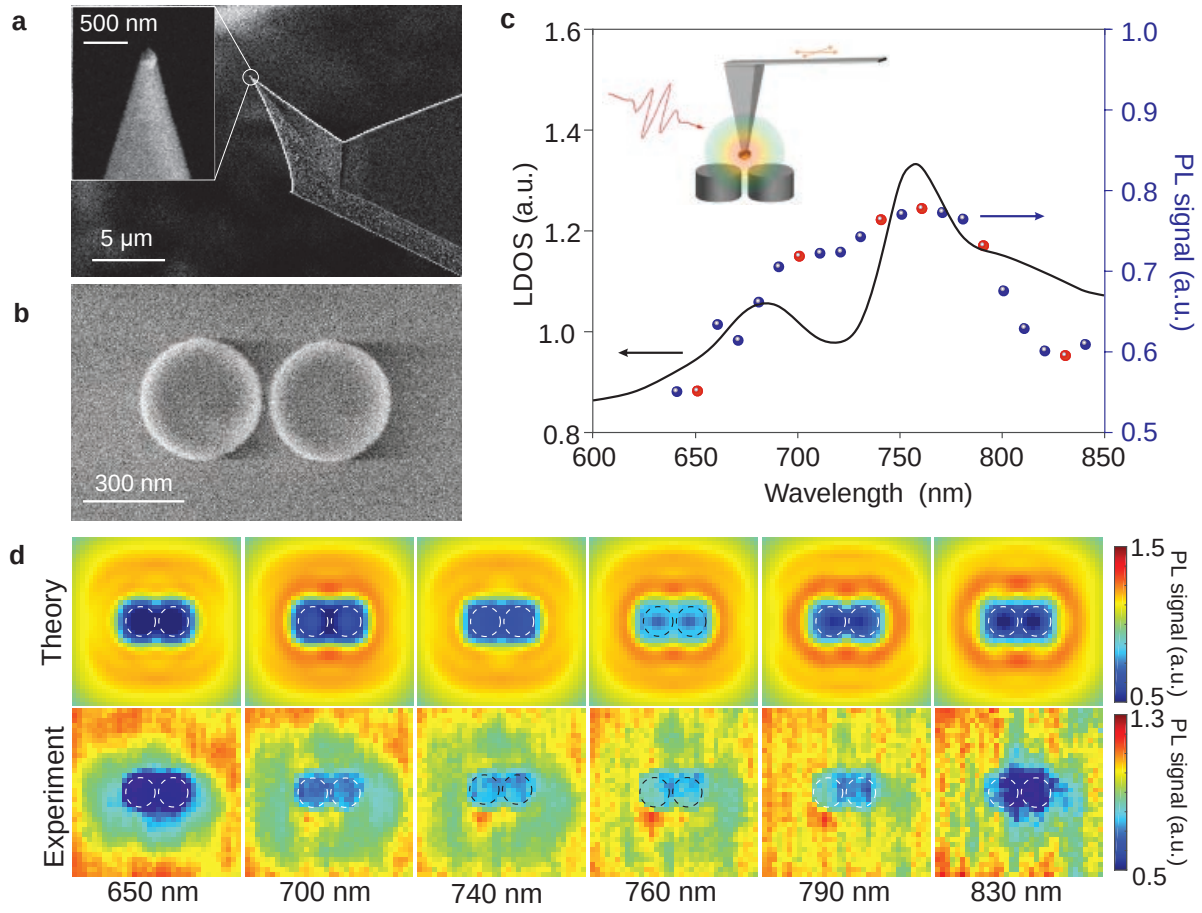

Figure 3: **Realization of ultrabroadband optical nanospectroscopy. (A)** SEM image of a tip of a Si cantilever functionalized with a Si/Au nanoparticle. **(B)** A dimer of a-Si:H nanodisks with height 165 nm, diameters 330 nm, and gap 40 nm. **(C)** Calculated (solid line) and measured (dots) mean PL signal above the dimer. Red dots correspond to experimental data presented in panel d. Inset: a sketch of the near-field setup. **(D)** Comparison of calculated (top row) and measured (bottom row) 2×2 μm^2 2D-maps of the PL enhancement near the dimer.

optical transitions (Fig. 2K) inefficient as compared to the energy relaxation. We propose several mechanisms that can explain hot PL in considered nanoparticles. (i) Nanosecond PL in the blue spectral range is known for Si nanocrystals and may originate from the Si–O, Si–H, or Si–C surface bonds (*11, 13, 21*) (Fig. 2L). (ii) Another mechanism of hot PL proposed in Ref. (*11*) is based on the Auger recycling processes (*22, 23*) that re-populate high-energy states of electrons and pump quasi-direct $\Gamma - \Gamma$ transitions (see Fig. 2I). Such hot PL emission exhibits redshift for smaller nanocrystals, and it broadens in an inhomogeneous ensemble. (iii) Hot carriers in silicon can also be generated due to ponderomotive acceleration by several consecutive pump pulses (*14*) (see Fig. 2J). (iv) Optically-induced heating of nanoparticle elevates the lattice temperature, and hence it leads to the Bose stimulation of optical phonon-assisted indirect emission, see Fig. 2K. Namely, the exciton emission rate in a nanocrystal is increased about 3 times at 1000 K (*24*). Moreover, (v) phonons emitted during the energy relaxation process in nanoparticles can be re-absorbed. This slows down the hot carrier energy relaxation by several times (*25*) and increases probability of light emission. (vi) Finally, we put forward the concept of plasmon-assisted hot PL emisison, see Fig. 2M. the proposed mechanism differs from the plasmonic Purcell-effect enhancement (*12*), and it is specific for indirect bandgap materials with free carriers, when the momentum mismatch between electrons and holes is compensated by plasmons rather than phonons.

For spatially separated plasmons and excitons, similar ideas were suggested in Refs. (*26, 27*). Here, the effect is stronger because all carriers are confined in the same nanoparticle. As shown in Ref. (*15*), for realistic concentrations of optically-induced electron-hole plasma (such as $\sim 10^{20}$ cm^{-3} (*28*)) the plasmon-assisted transitions are more efficient than phonon-assisted transitions by several orders of magnitude. This boosts hot PL efficiency explaining the observed broadband emission. All mentioned processes of hot PL emission can be attributed to the experimentally measured sub-ns times of the PL decay ($\tau_{hot}\approx$0.6 ns), whereas the observed

nanosecond-scale decay ($\tau_{hot}\approx$2.9 ns) can be assigned to defect-assisted processes.

For optimizing performance of the white-light emission from hybrid Si/Au nanoparticles, we find the range of incident intensities where the observed PL signal is stable, and its spectral shape does not depend on the intensity. According to Fig. 2E, the three-photon PL emission is observed for 2–10 GW/cm^2, whereas the dependence becomes quadratic for 10—30 GW/cm^2. Also, the SHG signal drops significantly for 8–20 GW/cm^2, as shown in Fig. 2E. A recovery of the SH signal is observed only for the intensities larger than 20 GW/cm^2. Since SHG in Si nanospheres requires nanocrystallinity for inducing local symmetry breaking (*29*), we relate the threshold-like decrease of the SH signal to annealing of the silicon part. Indeed, as follows from Fig. 2F, the out-coupling integral PL efficiency is saturated around the annealing threshold.

After uncovering the exceptional PL characteristics of the hybrid Si/Au nanoparticles, we employ a single nanoparticle as an ultrabroadband light source for near-field nanospectroscopy. To do so, we functionalize a common atomic force microscopy cantilever by attaching a hybrid nanoparticle to its very tip, as shown in Fig. 3A (for details, see Ref. (*15*)) similarly to the approach proposed in Ref. 10. The modified tip of the cantilever can then be irradiated by a laser light yielding localized white-light generation. The emitted light intensity is high enough, so that it is clearly visible with a microscope videocamera (see the inset in Fig. 1A and Supplementary Movie S1) and allows to measure the broadband spectra with subsecond acquisition time, which is critical for the implementation of ultrabroadband scanning optical nanospectroscopy.

As a test for near-field measurements, we consider a dimer consisting of two a-Si:H nanodisks with diameter 330 nm, see Fig. 3B. Such a structure is capable of providing the enhancement of both electric and magnetic fields at optical frequencies (*30*), and it is therefore well-suited for the demonstration of the concept of ultrabroadband nanospectroscopy enabled by nonlinear PL with hybrid nanoparticles. While measuring PL intensity in a broad spectrum range, we map the information about local PL enhancement in the vicinity of the silicon dimer

by scanning the functionalized AFM cantilever over the structure in the tapping mode (*15*).

To interpret the observed PL modifications, we employ a numerical model with a number of assumptions. First, we replace the emitting nanoparticle by point dipoles with three orthogonal orientations, which is a fair approximation taking into account its subwavelength size. We further assume that PL of the hybrid nanoparticle is incoherent, and we neglect the influence of the cantilever tip. Under these conditions, we model the measured PL maps as a sum of non-coherent radiation intensity of three mutually orthogonal dipole emitters scanned within a plane above the dimer. Owing to the experimental signal collection geometry, we only account for the emission of dipoles into the substrate. Spectral evolution of the PL maps near a silicon dimer is illustrated in Fig. 3(d). Both calculations (top row) and experimental data (bottom row) reveal conspicuous enhancement of the PL signal above the dimer near 760 nm wavelength. This is further supported by experimental and numerical spectra of normalized mean PL signal above the dimer shown in Fig. 3C, which demonstrate qualitative agreement with aperture-type NSOM (*4*), as shown in Fig.S7 (*15*).

Essentially, we demonstrate that hybrid nanoparticle attached to an AFM cantilever can be used as a nanoscale light source for probing the local optical properties of photonic nanostructures. However, as compared to other solutions for probes with embedded light sources, (*5–8*) the hybrid nanoparticle displays superior radiance combined with extremely broadband emission spectra, which offers unique versatility in near-field measurements.

In summary, we have demonstrated a bright white-light nanoscale source with the external quantum efficiency exceeding 0.1% based on hybrid Si/Au nanoparticles. The superb PL characteristics of the hybrid nanoparticles readily suggest multiple applications for probing the local optical properties of advanced nanoscale systems. The major advantage of the method utilizing nonlinear PL of nanoparticles is the possibility to measure the near-field response in a broad spectral range, essentially covering the whole visible spectrum, thus drastically decreasing the

required scanning time. This type of *"nanoscale light bulb"* can be employed as a versatile on-chip light source for broadband active media.

References

1. F. Lu, M. Jin, M. A. Belkin, *Nature Photonics* **8**, 307 (2014).
2. J. P. Hoogenboom, *et al.*, *Nano Letters* **9**, 1189 (2009).
3. H. A. Bechtel, E. A. Muller, R. L. Olmon, M. C. Martin, M. B. Raschke, *Proceedings of the National Academy of Sciences* **111**, 7191 (2014).
4. N. Rotenberg, L. Kuipers, *Nature Photonics* **8**, 919 (2014).
5. C. Ropp, *et al.*, *Nature Communications* **4**, 1447 (2013).
6. J. Michaelis, C. Hettich, J. Mlynek, V. Sandoghdar, *Nature* **405**, 325 (2000).
7. L. Aigouy, A. Cazé, P. Gredin, M. Mortier, R. Carminati, *Physical Review Letters* **113**, 076101 (2014).
8. R. Beams, *et al.*, *Nano Lett.* **13**, 3807 (2013).
9. J.-S. Bouillard, S. Vilain, W. Dickson, A. Zayats, *Optics Express* **18**, 16513 (2010).
10. D. Bouchet, *et al.*, *Physical Review Applied* **6**, 064016 (2016).
11. W. De Boer, *et al.*, *Nature Nanotechnology* **5**, 878 (2010).
12. C.-H. Cho, C. O. Aspetti, J. Park, R. Agarwal, *Nature Photonics* **7**, 285 (2013).
13. K. Dohnalová, *et al.*, *Light: Science & Applications* **2**, e47 (2013).
14. S. Sederberg, A. Y. Elezzabi, *Physical Review Letters* **113**, 167401 (2014).

15. Materials, methods and additional information are available as supplementary materials.

16. Y. He, *et al.*, *Journal of Applied Physics* **75**, 797 (1994).

17. R. A. Street, *Hydrogenated Amorphous Silicon* (Cambridge University Press, 2005).

18. M. W. Knight, H. Sobhani, P. Nordlander, N. J. Halas, *Science* **332**, 702 (2011).

19. R. Sundararaman, P. Narang, A. S. Jermyn, W. A. Goddard III, H. A. Atwater, *Nature Communications* **5** (2014).

20. R. Méjard, *et al.*, *ACS Photonics* **3**, 1482 (2016).

21. W. L. Wilson, P. Szajowski, L. Brus, *Science* **262**, 1242 (1993).

22. A. L. Efros, V. Kharchenko, M. Rosen, *Solid State Communications* **93**, 281 (1995).

23. M. Govoni, I. Marri, S. Ossicini, *Nature Photonics* **6**, 672 (2012).

24. T. Trupke, *et al.*, *Journal of Applied Physics* **94**, 4930 (2003).

25. A. A. Prokofiev, A. N. Poddubny, I. N. Yassievich, *Physical Review B* **89**, 125409 (2014).

26. J. Jung, M. L. Trolle, K. Pedersen, T. G. Pedersen, *Physical Review B* **84**, 165447 (2011).

27. M. Yamaguchi, K. Nobusada, *Physical Review B* **93**, 195111 (2016).

28. S. Makarov, *et al.*, *Nano Letters* **15**, 6187 (2015).

29. S. V. Makarov, *et al.*, *Nano Letters* **17**, 3047 (2017).

30. R. M. Bakker, *et al.*, *Nano Letters* **15**, 2137 (2015).

Acknowledgments

The authors thank A. Gudovskikh, A. Mozharov, E. Ubyvovk, and G. Zograf for assistance with samples and experiments, and also M. Belkin, T. Gregorkiewicz, S. Kruk, K. Kuipers, and M. Stockman for their interest to this work and useful comments. The work was supported by the Russian Foundation for Basic Research (grants 17-03-00621, 17-02-00538, 16-29-05317, 16-02-00684), Russian Ministry of Education and Science (Projects 16.8939.2017/8.9, 3.8891.2017/8.9, and 2.2267.2017/4.6), the Australian Research Council, and A*STAR SERC Pharos program, Grant No. 152 73 00025 (Singapore).